ATMOSPHERE

Sunlight drives the abiotic formation of nitrous oxide in fresh and marine waters

Elizabeth Leon-Palmero[1,2]*†, Rafael Morales-Baquero[1], Bo Thamdrup[2], Carolin Löscher[2], Isabel Reche[1,3]

Nitrous oxide (N_2O) is a potent greenhouse gas and the main stratospheric ozone-depleting agent, yet its sources are not well resolved. In this work, we experimentally show a N_2O production pathway not previously considered in greenhouse gas budgets, which we name photochemodenitrification. Sunlight induces substantial and consistent N_2O production under oxic abiotic conditions in fresh and marine waters. We measured photochemical N_2O production rates using isotope tracers and determined that nitrite is the main substrate and that nitrate can also contribute after being photoreduced to nitrite. Additionally, this N_2O production was strongly correlated to the radiation dose. Photochemodenitrification exceeded biological N_2O production in surface waters. Although previously overlooked, this process may contribute considerably to global N_2O emissions through its occurrence in fresh and marine surface waters.

Nitrous oxide (N_2O) is the main stratospheric ozone-depleting agent (*1*) and one of the strongest greenhouse gases—about 273 times as potent as carbon dioxide (*2*). Since preindustrial times, the concentration of atmospheric N_2O has risen by 23% (*2*), in a trend strongly correlated to the higher bioavailability of reactive nitrogen (N) in the environment, largely owing to industrial N fixation by the Haber–Bosch process (*3*). A considerable portion of the anthropogenic N applied to land as fertilizers enters rivers, estuaries, and continental shelves, which boosts the production and emission of N_2O in these aquatic systems (*4*–*6*). These emissions resulting from N inputs—estimated to 0.5 Tg of N $year^{-1}$ for the 2007 to 2016 period—exceed natural emissions from inland waters, estuaries, and coastal zones [0.3 Tg N $year^{-1}$ (*7*)]. The rate of increase in atmospheric N_2O during the past decade was even faster than predicted by the Intergovernmental Panel on Climate Change (IPCC) (*8*), which emphasizes the need for better identification of the sources of N_2O to reduce uncertainty in climate assessments and optimize mitigation strategies (*7*).

Ammonia oxidation and denitrification are the microbial processes that are assumed to control the N_2O budget in aquatic ecosystems. Ammonia-oxidizing archaea (AOA) and bacteria (AOB) release N_2O in well-oxygenated waters as a side product during ammonia oxidation to nitrite (NO_2^-) (*9*). N_2O is also an intermediate product during denitrification of NO_3^- and NO_2^- to N_2O and N_2, a process that is usually coupled to organic matter oxidation and occurs under oxygen-depleted conditions (*10*). Both microbial processes have been extensively studied in the water column and sediments of aquatic ecosystems. Abiotic processes, such as chemodenitrification, can also contribute to the production of N_2O in soils and marine sediments (*11*, *12*). During chemodenitrification, NO_3^- and NO_2^- are abiotically reduced to N_2O coupled to the oxidation of metals, such as Fe (II), or organic matter (*11*). However, the abiotic production of N_2O within the water column of fresh waters and marine ecosystems remains largely unexplored, particularly in surface waters. Processes occurring in the upper meters of the well-mixed layer hold the potential for a disproportionate contribution to N_2O emissions owing to their closeness to the atmosphere, which may facilitate the air-sea exchange of N_2O when oversaturated. In this work, we describe the discovery of a photochemical source of N_2O, which we named photochemodenitrification. We detected this reaction, mediated by sunlight, that uses NO_2^- as substrate in two freshwater reservoirs and two coastal marine systems, demonstrating that it may represent an unrecognized but widespread process relevant to global budgets.

Photochemical formation of N_2O

In a previous study, we found recurrently higher N_2O emissions during the daytime versus during the nighttime during 24-hour flux measurement campaigns over the course of 2 years in two freshwater reservoirs in southeast Spain (Cubillas and Iznájar). Despite differences in magnitude among years and reservoirs, this pattern in N_2O emissions was consistent and significantly correlated to the solar cycle, with daytime emissions up to one order of magnitude greater than nighttime emissions (*13*). However, that pattern was inconsistent with classical microbial production through ammonia oxidation, which is in-

[1]Departamento de Ecología, Universidad de Granada, Granada, Spain. [2]Nordcee, Department of Biology, University of Southern Denmark, Odense, Denmark. [3]Research Unit Modeling Nature (MNat), Universidad de Granada, Granada, Spain.
*Corresponding author. Email: el23@princeton.edu
†Present address: Department of Geosciences, Princeton University, Princeton, NJ, USA.

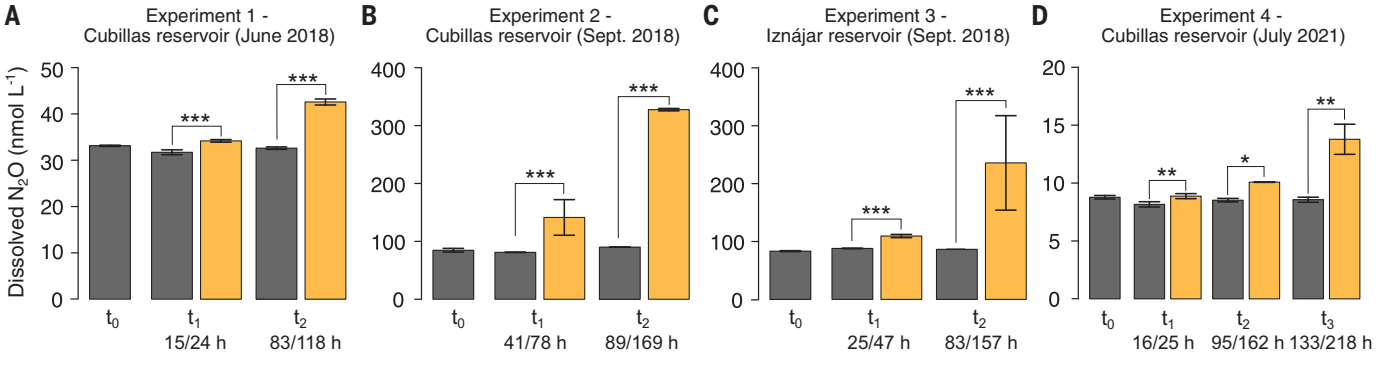

Fig. 1. Effect of sunlight on N_2O production. Dissolved N_2O concentrations over time (i.e., daylight time/total incubation hours) in the incubation experiments 1 to 4. (**A**) Cubillas in June 2018, unfiltered water. (**B**) Cubillas in September 2018, unfiltered water. (**C**) Iznájar in September 2018, unfiltered water. (**D**) Cubillas in July 2021, filtered water (0.7 μm pore size). $HgCl_2$ (1 mmol $liter^{-1}$) was added in all experiments to inhibit biological activity. Bars represent the mean values ± standard errors over the time course (t_0 to t_3), including dark controls (dark gray bars) and sunlight treatments (yellow bars). Sunlight exposure time/total incubation hours are shown (e.g., 15/24 hours). Note the different scales in the *y* axes. The significance of the sunlight treatments is included for each experiment: $*P < 0.05$; $**P < 0.01$; $***P < 0.001$. Rates are presented in table S2. More statistical details are provided in table S3.

hibited by light (*14*), or through denitrification, which requires oxygen depletion (*15*, *16*). We hypothesized that sunlight may induce the photochemical production of N_2O in surface waters, boosting the fluxes during the daytime. To investigate this hypothesis, we first performed four incubation experiments, exposing surface water from Cubillas and Iznájar reservoirs to natural sunlight with inhibition of biological activity by the addition of $HgCl_2$ (experiments 1 to 4; table S1). We used ultraviolet (UV)–transparent quartz vials and included dark controls during the incubations. All experiments were conducted under natural, oxic conditions (more details are provided in the materials and methods and fig. S1). The incubation experiments performed during this study and the initial inorganic N pools are listed in table S1.

We detected a significant, consistent, and continuous increase in the N_2O concentration in the sunlight treatments in the four incubation experiments relative to the dark controls (Fig. 1; experiments 1 to 4). Photochemical N_2O production was detected in both the experiments performed using unfiltered (experiments 1 to 3) and filtered water (0.7 μm pore size; experiment 4), with rates varying from 1.01 ± 0.22 nmol N-N_2O liter^{-1} day^{-1} in experiment 4 to 66.6 ± 15.1 nmol N-N_2O liter^{-1} day^{-1} in experiment 2 (table S2). The photochemical N_2O production rate measured in experiment 4 was equivalent to $2.6 \times 10^{-9} \pm 5.5 \times 10^{-10}$ nmol-N W^{-1} photosynthetically active radiation (PAR) and to $2.3 \times 10^{-5} \pm 4.6 \times 10^{-6}$ nmol-N W^{-1} UVB received. In relation to the in situ N_2O concentration, the daily relative increase varied from 3.8% (initial concentration = 13.4 nmol liter^{-1}) in experiment 4 to 39.3% (initial concentration = 84.6 nmol liter^{-1}) in experiment 2 (table S2), thus contributing substantially to the N_2O pool.

Previous studies in rivers have reported higher N_2O emissions or concentrations during the daytime versus the nighttime (*17*–*20*), although the opposite has also been shown (*21*, *22*). These patterns have been attributed to changes in N cycling by biological activity and water temperature (*17*–*21*). Liu *et al.* (*23*) found that the seasonal pattern in N_2O fluxes in Antarctic lakes was positively related to daily radiation, concluding that the increase of daily radiation may favor photosynthesis and thus stimulate N_2O production from the decomposition of the algae. The experiments presented in this work indicate that solar radiation directly drives an abiotic production of N_2O that may represent an important source of N_2O to the atmosphere that has not been reported previously or considered in greenhouse gas budgets. Solar radiation, mostly in the UV band (280 to 400 nm), catalyzes many photochemical reactions in fresh and marine surface waters, including the decomposition of chromophoric and recalcitrant organic molecules (*24*); the reduction of metals, such as iron (*25*, *26*) or manganese (*27*); the photochemical production of climate-relevant gases, such as carbon dioxide (*28*), carbon monoxide (*29*), and methane (*30*); and the photolysis of NO_3^- and NO_2^- (*31*–*33*). The discovery presented in this work indicates that solar radiation can also catalyze the production of N_2O in surface waters, and its importance—not only for daily variability but also as a source of N_2O to the atmosphere—should be addressed.

Table 1. Summary of the rates of photochemodenitrification and biological N_2O production from ammonia oxidation. When derived from ^{15}N labeling experiments, the total rates of N_2O production were obtained by adding the rates from $^{15}N\text{-}NO_2^-$ and from $^{15}N\text{-}NO_3^-$. The incubation experiments to measure biological N_2O production were performed in darkness, except experiment 7, which included darkness and natural day-night cycle treatments. More details are presented in tables S2, S6, and S8. Dashes indicate not applicable.

Site (experiment)	Total N_2O from photochemodenitrification (nmol N-N_2O liter^{-1} day^{-1})		N_2O from ammonia oxidation (nmol N-N_2O liter^{-1} day^{-1})	
Cubillas and Iznájar reservoirs (experiments 1 to 4 and 9)	June 2018 (exp. 1, Cubillas)	2.96 (±0.20)	July 2018 (exp. 9)	0.83 (±0.00): Iznájar; 2.08 (±0.15): Cubillas
	September 2018 (exp. 2, Cubillas)	66.56 (±15.11)	September 2018 (exp. 9)	0.06 (±0.00), 0.47 (±0.12): Cubillas; 0.93 (±0.25): Iznájar
	September 2018 (exp. 3, Iznájar)	47.86 (±17.44)		
	July 2021 (exp. 4, Cubillas)	1.01 (±0.22)	–	–
Cubillas reservoir (experiment 5)	July 2021	2.32 (±0.22)	–	–
Motril coast (experiment 6)	July 2021	1.41 (±0.06)	–	–
Boknis Eck (experiment 7)	July 2022	0.03 (±0.00)	July 2022	0.015 (±0.002) (darkness); 0.007 (±0.002) (day-night cycle)

Nitrite and sunlight explain N_2O photochemodenitrification

We hypothesized that NO_2^- may act as a substrate for photochemical N_2O production based on our data from experiments 1 to 4 (fig. S2). A marginally significant relationship between the in situ NO_2^- concentrations and the photochemical N_2O production rates was found (n = 4 observations, $P < 0.1$; fig. S2A). Additionally, we detected a significant decrease in the NO_2^- concentration to below detection (0.5 μmol liter^{-1}) in the sunlight treatments compared with the dark controls during experiment 4 ($P < 0.001$; fig. S2B). We tested our hypothesis by adding $^{15}N\text{-}NO_2^-$ or $^{15}N\text{-}NO_3^-$ to trace the formation of $^{15}N\text{-}N_2O$ [as $^{45}N_2O$ ($^{14}N^{15}N^{16}O$) and $^{46}N_2O$ ($^{15}N^{15}N^{16}O$); experiments 5 to 7], expanding our analysis to include two marine systems at different latitudes (Motril coast and Boknis Eck, experiments 6 and 7, respectively) in addition to a freshwater system (Cubillas reservoir, experiment 5; see table S1 for study site details and fig. S1 for the experimental setup). We included the treatment with $^{15}N\text{-}NO_3^-$ because NO_3^- is generally the most abundant form of dissolved inorganic N in these systems, and NO_2^- derived from its abiotic photolysis (*31*) may serve as a substrate for photochemical production of N_2O.

We detected a significant production of $^{15}N\text{-}N_2O$ from $^{15}N\text{-}NO_2^-$ in the sunlight treatments in the three study systems, with longer sunlight exposure yielding more N_2O (Fig. 2, A to C, and fig. S3). Significant production of $^{15}N\text{-}N_2O$ from $^{15}N\text{-}NO_3^-$ was also observed in experiments 5 and 6 (Fig. 2, D and E, and fig. S3), although the rate of N_2O production from $^{15}N\text{-}NO_3^-$ was at least one order of magnitude lower than that from $^{15}N\text{-}NO_2^-$. These results support our hypothesis that NO_2^- is the direct and main substrate for this reaction. In turn, NO_3^- must be photoreduced to NO_2^- to later produce N_2O in a second step. On the basis of these findings, we named the reaction photochemodenitrification. The photochemical process generated both single- and double-labeled N_2O ($^{45}N_2O$ and

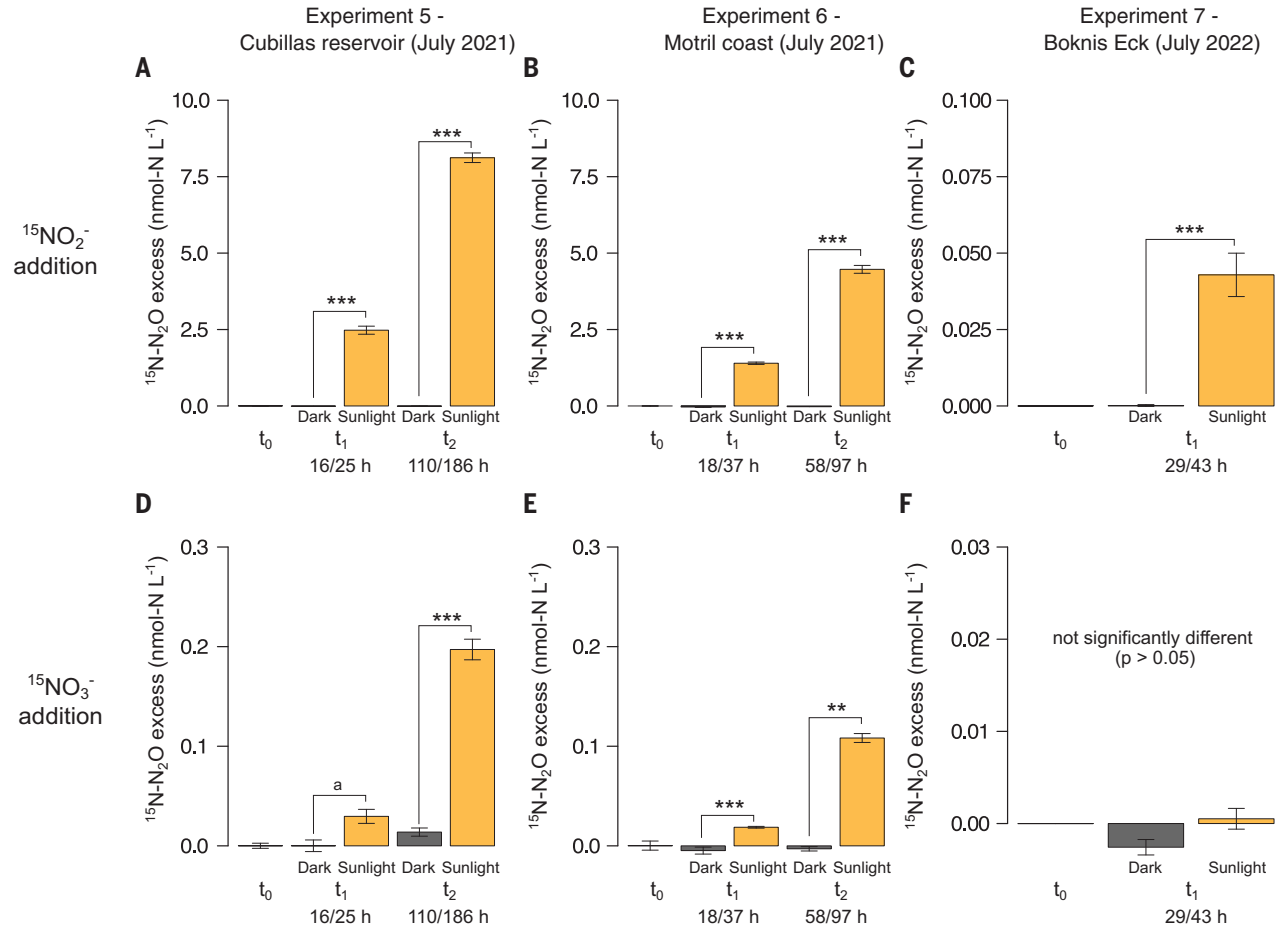

Fig. 2. Photochemical production of ^{15}N-N_2O from ^{15}N-NO_2^- and ^{15}N-NO_3^-. (**A** to **F**) ^{15}N-N_2O excess (in nanomoles of N per liter) calculated with respect to t_0, over incubation time (sunlight hours/total hours) in the experiments in the Cubillas reservoir (filtered water, 0.7 μm pore size) [(A) and (D)], the Motril coast (filtered water, 0.7 μm pore size) [(B) and (E)], and Boknis Eck (unfiltered water) [(C) and (F)], from ^{15}N-NO_2^- [(A) to (C)] and ^{15}N-NO_3^- [(D) to (F)]. $HgCl_2$ (1 mmol liter^{-1}) was added in all experiments to inhibit biological activity. Bars represent the mean values ± standard errors over the time course (t_0 to t_2), including dark controls (dark gray bars) and sunlight treatments (yellow bars). Note the different scales in the *y* axes. The significance of the sunlight treatments is included for each experiment: *a* indicates $P < 0.1$; $^{**}P < 0.01$; $^{***}P < 0.001$. Photochemical production rates as a function of the bottle area, volume, and radiation doses are presented in table S6, and the statistical details are provided in table S4.

$^{46}N_2O$) from both tracers (fig. S3). This is broadly consistent with the isotope pairing expected from the production of N_2O from a mixture of added $^{15}NO_2^-$ and unlabeled nitrite (^{14}N-NO_2^-) from either the initial in situ pool or formed, for example, from NO_3^- photolysis (fig. S4). The contribution of other forms of in situ organic or inorganic N compounds as sources of ^{14}N to the formation of $^{45}N_2O$ cannot be excluded (see the supplementary text for further explanation).

Photochemodenitrification depended linearly on the sunlight radiation received (Fig. 3 and table S5). We found similar radiation normalized rates (i.e., the slope in the increase in N_2O per radiation dose) across experiments, whether based on UVB or PAR (Fig. 3 and table S5). In experiment 4, in which we did not add any tracer (Fig. 3A), the slopes for PAR ($S_{PAR} = 5.9 \times 10^{-6} \pm 1.2 \times 10^{-6}$) and UVB radiation ($S_{UVB} = 0.051 \pm 0.010$) were not significantly different from the slopes calculated for the $^{15}NO_2^-$ additions in experiments 5 to 7 (Fig. 3B; $S_{PAR} = 6.3 \times 10^{-6} \pm 2.4 \times 10^{-7}$ and $S_{UVB} = 0.054 \pm 0.002$). In agreement with our previous results, the slopes were one order of magnitude lower for the $^{15}NO_3^-$ additions (Fig. 3C).

Rates of photochemical production of ^{15}N-N_2O in the ^{15}N-NO_2^- addition experiments varied from 0.03 ± 0.00 nmol-N liter^{-1} day^{-1} in Boknis Eck (experiment 7) to 2.03 ± 0.18 nmol-N liter^{-1} day^{-1} in the Cubillas reservoir (experiment 5; table S6). Photochemical production rates from ^{15}N-NO_3^- were similar in the Motril coast (0.26 ± 0.02 nmol-N liter^{-1} day^{-1}) and the Cubillas reservoir (0.29 ± 0.04 nmol-N liter^{-1} day^{-1}) (experiments 5 and 6; table S6). With both ^{15}N-NO_2^- and ^{15}N-NO_3^-, the photochemical N_2O production rates measured in the Cubillas reservoir (experiment 5) and the Motril coast (experiment 6) were larger than in Boknis Eck (experiment 7; Fig. 2 and table S6). The higher substrate availability and higher radiation doses in experiments 5 and 6 versus those in experiment 7 could have caused these differences. We used higher concentrations of ^{15}N-labeled tracers in experiments 5 and 6 compared with experiment 7 (i.e., 2 to 5 μmol liter^{-1} versus 0.5 μmol liter^{-1}) to reflect the natural differences in NO_3^- and NO_2^- concentrations found in these systems (table S1). In addition, the lower production detected in experiment 7 compared with experiments 5 and 6 may also be related to the lower radiation received in this experiment (Fig. 3), which was incubated in Odense, Denmark (~55°N, 57-m altitude), whereas the others were incubated in Granada,

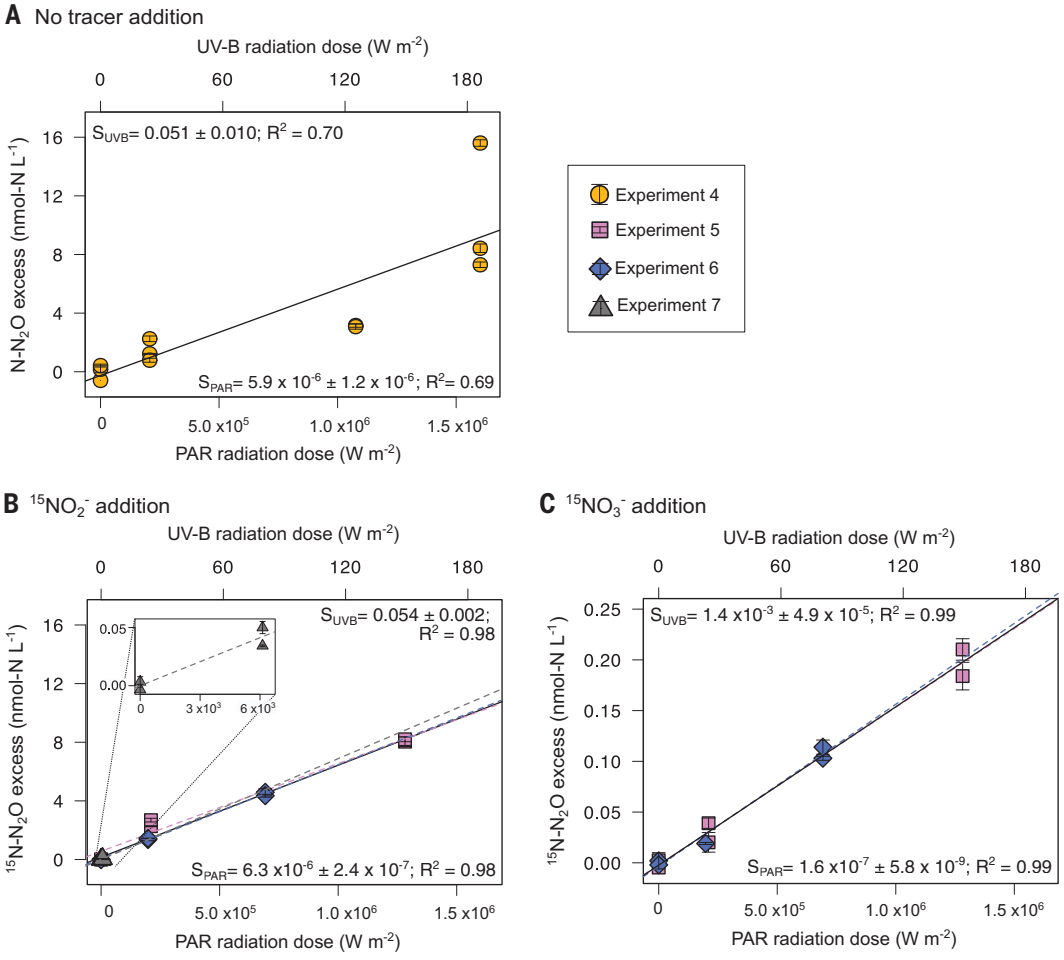

Fig. 3. Photochemical production of N_2O as function of UVB and PAR dose. Linear increases in the concentrations of $^{(15)}N$ in the N_2O pool relative to the initial abundance (N_2O excess, in nanomoles of N per liter) in experiments 4 to 7. (**A**) No tracer addition. (**B**) $^{15}NO_2^-$ addition. (**C**) $^{15}NO_3^-$ addition. The combined slopes (S_{PAR} and S_{UVB}) are shown in the figure, and the individual slopes for each experiment are provided in table S5. Note the zoom-in plot in (B) and the different scales in the *y* axes. We did not measure UVB or PAR during experiments 1 to 3.

Spain (~37°N, 738-m altitude). Despite the lower radiation dose received, which determined the lower ^{15}N-N_2O production, the radiation-normalized rates were similar in the three systems at different latitudes (Fig. 3 and table S5). UV radiation, which may be causing this reaction, tends to increase as we approach the equator and ascend in altitude. Sunlight hours per day also change with the time of the year and latitude, but this variation was accounted for by considering the exact number of sunlight hours in the rate calculations. In addition to the experimental evidence, we also found that the photochemical N_2O production rates were a function of in situ NO_2^- concentration ($P < 0.05$), following an exponential fit [N-N_2O production = $0.32e^{0.23(\text{nitrite})}$ (where e is Euler's number), adjusted coefficient of determination (R^2) = 0.65; Fig. 4]. This finding supports the hypothesis that NO_2^- plays an active role in the photochemical formation of N_2O.

We performed a final experiment to rule out the potential impact of the biocide $HgCl_2$ on the photochemical production of N_2O (experiment 8; fig. S5 and table S7). Water was gently prefiltered once (1.0 μm), and sterile filtered twice (0.2 μm) to remove the organisms present in the sample. Then, parallel treatments were incubated with and without $HgCl_2$. We detected a significant increase in the ^{15}N-N_2O concentration after sunlight exposure in both treatments. N_2O production in sunlight conditions was 54% larger ($P < 0.05$) in the treatment without $HgCl_2$ than in the treatment with $HgCl_2$, and no production was detected in dark conditions. Although unlikely, we cannot exclude that the difference may be the result of biological reactions by cells smaller than 0.2 μm. However, if that were the case, we would likely have detected production in the dark controls without $HgCl_2$, but we did not detect any production in those controls. Based on these results, it is very unlikely that $HgCl_2$ causes the photochemical N_2O production. If anything, $HgCl_2$ addition may reduce photochemical N_2O production rather than increase it.

Our data show experimental (experiments 1 to 7; Figs. 1 and 2) and in situ evidence (Fig. 4) that NO_2^- and NO_3^- are substrates for the photochemical production of N_2O and that this process significantly depends on sunlight exposure (Fig. 3). NO_2^- and especially NO_3^- are abundant compounds in eutrophic aquatic systems, such as many freshwater bodies and wetlands, as well as coastal areas and estuaries, which are strongly influenced by N loading from their watersheds (*34*, *35*) and act as global hotspots for N_2O production (*4*, *6*, *36*). For instance, NO_2^- and NO_3^- concentrations reached up to 11 μmol liter^{-1} and >300 μmol liter^{-1}, respectively, in the surface water column of Mediterranean reservoirs (*34*) and >2 μmol liter^{-1} in the surface waters of the Chesapeake Bay estuary (*37*). In the open ocean, inorganic N concentrations in surface waters vary from region to region. They are typically low in oligotrophic tropical and subtropical regions, where nutrient uptake by phytoplankton is high and upwelling is less common. However, concentrations are higher in upwelling zones and polar regions, where annual average surface values of NO_3^- are ~5 to 25 μmol liter^{-1} (*38*).

Therefore, photochemical N_2O production rates are expected to be substantial in regions with greater availability of inorganic N and lower in oligotrophic waters, which generally correlates with patterns in N_2O concentration and biological N_2O production (*4*, *6*, *7*, *36*, *39*). We hypothesize that other biological reactions, such as ammonia oxidation, and/or abiotic processes, such as the photodegradation of dissolved organic matter, which release NO_2^- and other forms of inorganic N (*40*), may enhance photochemical N_2O production. If production

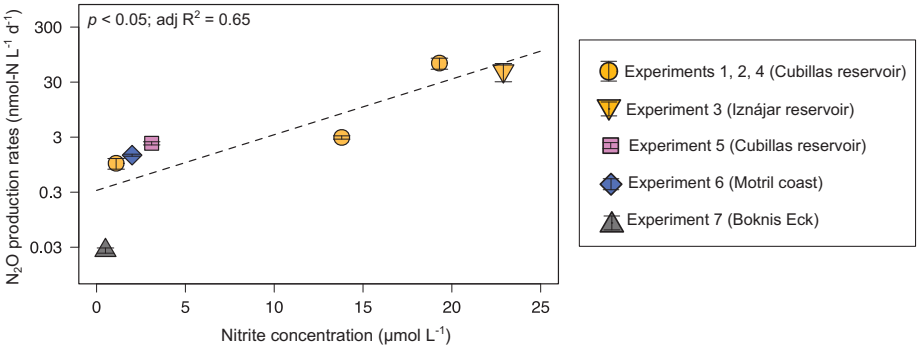

Fig. 4. Total N_2O photochemical production rates as a function of the in situ nitrite concentration. N_2O photochemical production rates (in nanomoles of N per liter per day) ± standard errors are represented. Note the log scale in the *y* axis. The N_2O photochemical production rate measured in the Cubillas reservoir in June 2018 (sampling performed on 22 June) was related to the nitrite concentration measured in the Cubillas reservoir on 4 July 2018. In experiments 5 to 7, we added the nitrite used as tracer to the in situ nitrite concentration.

and consumption are tightly coupled, they might create a cryptic cycle in which the NO_2^- remains undetected. This effect may be particularly important in oligotrophic waters. The contribution of other sources of NO_2^- or forms of N may contribute to explain the results found in Boknis Eck (experiment 7), in which a higher production of $^{45}N_2O$ compared with $^{46}N_2O$ was detected, despite in situ NO_2^- and NO_3^- concentrations being below detection levels. This result suggests that other forms or sources of organic or inorganic in situ N compounds may contribute ^{14}N to the formation of $^{45}N_2O$ (fig. S3 and supplementary text).

The photochemical reduction of NO_2^- to N_2O during photochemodenitrification may be coupled to the oxidation of organic matter or metals, such as Fe or Mn, similar to chemodenitrification (*11*, *12*, *41*). These metals experience photoreduction in surface waters (*25*, *27*, *42*). Alternatively, N_2O may also be produced through UV light–catalyzed photolysis (*33*, *43*, *44*). Additional research is needed to elucidate the ultimate mechanism of this process.

Photochemical processes rely mostly on UV radiation, including UVB (280 to 315 nm) and UVA (315 to 400 nm), which is rapidly attenuated in the water column. For instance, NO_3^- photolysis occurs in the UVB band, centered at 302 nm, whereas NO_2^- photolysis occurs in the UVB and UVA bands, with an absorption maximum at 354 nm (*33*). Longer wavelengths carry less energy and penetrate deeper into the water column. Vanderploeg *et al.* found that 1% of the UV radiation penetrated from 2 to 4 m for UVB (305 nm) and between 11 and 22 m for UVA (395 nm) in Lake Michigan (*45*). By contrast, there is still about 10% of the surface radiation at depths between 6 and 31 m (UVB) and between 15 and 104 m (UVA) in the oligotrophic ocean (*46*). In more eutrophic water bodies, sunlight attenuation is typically high; yet, the likely greater availability of inorganic N in these systems may compensate for the total depth-integrated photochemical production rates (Fig. 4). Solar radiation also changes with latitude and altitude. Therefore, N_2O production by photochemodenitrification may present a latitudinal pattern in the global ocean and fresh waters related to the differences in solar radiation and influenced by NO_2^- and NO_3^- concentrations around the globe.

Photochemodenitrification versus biological N_2O production

The N_2O production rates from photochemodenitrification exceeded the biological N_2O production from ammonia oxidation, which has been classically considered the key N_2O production process in surface waters (Table 1). Biological production of ^{15}N-N_2O from ammonia oxidation varied from 0.06 ± 0.00 nmol N-N_2O liter^{-1} day^{-1} in Iznájar to 2.08 ± 0.15 nmol N-N_2O liter^{-1} day^{-1} in Cubillas (experiment 9; Table 1). These biological rates were determined by incubating the samples in darkness. In Boknis Eck, biological production of ^{15}N-N_2O reached up to 0.015 ± 0.002 nmol N-N_2O liter^{-1} day^{-1} when the samples were incubated in darkness and 0.007 ± 0.002 nmol N-N_2O liter^{-1} day^{-1} when the samples were incubated in natural day-night conditions (Table 1). We did not find a significant relationship between N_2O production rates by ammonia oxidation and the in situ N_2O concentration in the study reservoirs (fig. S6). However, we found that in situ N_2O concentration was a function of the photochemical N_2O production rates ($n = 5$, $P < 0.01$; fig. S6). Therefore, the production of N_2O by photochemodenitrification may contribute substantially to sustaining the recurrent surface N_2O supersaturation found in fresh waters (*34*) and potentially in marine ecosystems, including coastal areas (*37*) and the open ocean (*47*), where the production of N_2O from ammonia oxidation in surface waters is typically low.

The rates of N_2O photochemodenitrification detected were higher than the N_2O production by ammonia oxidation in coastal and open ocean regions (*37*, *47*) but lower than those found for N_2O production by denitrification in rivers (*48*). They were similar to the N_2O production rates by phytoplankton cultures (*49*). Moreover, ammonia oxidation rates are typically measured in the dark, which eliminates possible contributions with photochemical processes. Because ammonia oxidizers are sensitive to light (*14*), this may overestimate the biological N_2O production rates in surface waters, as illustrated by our finding of higher rates in darkness compared with natural day-night conditions (experiment 7; Table 1). Still, the photochemical N_2O production rate was at least twice the biological N_2O production in darkness.

N_2O production by photochemodenitrification represents a substantial contribution to the N_2O pool in freshwater reservoirs and may also represent a considerable contribution in coastal marine waters. The fact that N_2O production by photochemodenitrification exhibits its maximum at the very surface of the water, which is in direct contact with the atmosphere, suggests that this reaction may have a disproportionate effect on N_2O fluxes. This is because the newly formed N_2O may diffuse more quickly to the atmosphere when oversaturated compared with the N_2O produced and stored deeper in the water column. Our findings could also imply that the emission of N_2O from surface waters may be larger than previously estimated, particularly by biogeochemical models (*36*, *50*). The recent global synthesis on N_2O fluxes by Resplandy *et al.* (*36*) showed that global ocean biogeochemical model emission estimates for coastal waters are lower than those based on observations (*39*). This may indicate that these biogeochemical models underestimate emissions because they do not account for all N_2O sources. We suggest that this underestimation could be, at least partially, related to photochemical N_2O production.

The N_2O production pathway presented in this work (fig. S7) represents a previously unrecognized but potentially relevant source of N_2O for future emission budgets. This reaction may be particularly important for eutrophic freshwater bodies, coastal areas, and upwelling marine regions, which are global N_2O emission hotspots (*4*, *6*, *7*, *36*). In the coming decades, N_2O emissions may be further amplified by the projected increase in global N export to fresh waters and coastal environments resulting from the growing population (*35*). This increase may lead to higher rates of photochemical N_2O formation. Therefore, it is crucial to include this pathway in future assessments. This discovery represents a breakthrough in the study of global sources of N_2O, helping to reduce the current uncertainties in the bottom-up estimates highlighted in the last global N_2O inventories (*7*) and

to explain accelerating emissions, which exceed some of the highest projected scenarios (*8*).

REFERENCES AND NOTES

1. A. R. Ravishankara, J. S. Daniel, R. W. Portmann, *Science* **326**, 123–125 (2009).
2. Intergovernmental Panel on Climate Change (IPCC), *Climate Change 2021 – The Physical Science Basis: Working Group I Contribution to the Sixth Assessment Report of the Intergovernmental Panel on Climate Change* (Cambridge Univ. Press, 2023).
3. N. Gruber, J. N. Galloway, *Nature* **451**, 293–296 (2008).
4. S. P. Seitzinger, C. Kroeze, R. V. Styles, *Chemosphere Glob. Change Sci.* **2**, 267–279 (2000).
5. E. León-Palmero, R. Morales-Baquero, I. Reche, *Environ. Res. Lett.* **15**, 044012 (2020).
6. Y. Li *et al*., *Nat. Commun.* **15**, 942 (2024).
7. H. Tian *et al*., *Nature* **586**, 248–256 (2020).
8. R. L. Thompson *et al*., *Nat. Clim. Change* **9**, 993–998 (2019).
9. B. B. Ward, "Nitrification" in *Encyclopedia of Ecology*, vol. 2, B. Fath, Ed. (Elsevier, ed. 2, 2013), pp. 351–358.
10. B. B. Ward, *Science* **341**, 352–353 (2013).
11. X. Zhu-Barker, A. R. Cavazos, N. E. Ostrom, W. R. Horwath, J. B. Glass, *Biogeochemistry* **126**, 251–267 (2015).
12. S. D. Wankel *et al*., *Nat. Commun.* **8**, 15595 (2017).
13. E. León-Palmero, R. Morales-Baquero, I. Reche, bioRxiv 2023.10.24.563772 [Preprint] (2023).
14. S. N. Merbt *et al*., *FEMS Microbiol. Lett.* **327**, 41–46 (2012).
15. P. Bonin, M. Gilewicz, J. C. Bertrand, *Can. J. Microbiol.* **35**, 1061–1064 (1989).
16. T. Dalsgaard *et al*., *mBio* **5**, e01966 (2014).
17. J. A. Harrison, P. A. Matson, S. E. Fendorf, *Aquat. Sci.* **67**, 308–315 (2005).
18. T. J. Clough, L. E. Buckthought, F. M. Kelliher, R. R. Sherlock, *Glob. Change Biol.* **13**, 1016–1027 (2007).
19. L. Yang, W. Yan, P. Ma, J. Wang, *J. Geogr. Sci.* **21**, 820–832 (2011).
20. H. M. Baulch *et al*., *Freshw. Biol.* **57**, 509–525 (2012).
21. M. S. Rosamond, S. J. Thuss, S. L. Schiff, R. J. Elgood, *J. Environ. Qual.* **40**, 256–270 (2011).
22. R. L. Woodrow *et al*., *Limnol. Oceanogr. Lett.* **9**, 276–285 (2024).
23. Y. Liu *et al*., *Atmos. Environ.* **45**, 1464–1475 (2011).
24. I. Reche, M. L. Pace, J. J. Cole, *Ecosystems* **3**, 419–432 (2000).
25. L. Emmenegger, R. Schönenberger, L. Sigg, B. Sulzberger, *Limnol. Oceanogr.* **46**, 49–61 (2001).
26. K. Barbeau, E. L. Rue, K. W. Bruland, A. Butler, *Nature* **413**, 409–413 (2001).
27. W. G. Sunda, S. A. Huntsman, G. R. Harvey, *Nature* **301**, 234–236 (1983).
28. B. Koehler, T. Landelius, G. A. Weyhenmeyer, N. Machida, L. J. Tranvik, *Global Biogeochem. Cycles* **28**, 696–711 (2014).
29. L. Conte, S. Szopa, R. Séférian, L. Bopp, *Biogeosciences* **16**, 881–902 (2019).
30. Y. Li, C. G. Fichot, L. Geng, M. G. Scarratt, H. Xie, *Geophys. Res. Lett.* **47**, e2020GL088362 (2020).
31. O. C. Zafiriou, M. B. True, *Mar. Chem.* **8**, 33–42 (1979).
32. O. C. Zafiriou, M. B. True, *Mar. Chem.* **8**, 9–32 (1979).
33. J. J. Jankowski, D. J. Kieber, K. Mopper, *Photochem. Photobiol.* **70**, 319–328 (1999).
34. E. León-Palmero, R. Morales-Baquero, I. Reche, *Limnol. Oceanogr.* **68**, 1734–1749 (2023).
35. A. H. W. Beusen *et al*., *Glob. Environ. Change* **72**, 102426 (2022).
36. L. Resplandy *et al*., *Glob. Biogeochem. Cycles* **38**, e2023GB007803 (2024).
37. W. Tang *et al*., *Limnol. Oceanogr.* **67**, 2101–2116 (2022).
38. EU Copernicus Marine Service information (CMEMS), "Global Ocean Biogeochemistry Analysis and Forecast" (Marine Data Store, 2025); https://doi.org/10.48670/moi-00015.
39. S. Yang *et al*., *Proc. Natl. Acad. Sci. U.S.A.* **117**, 11954–11960 (2020).
40. R. J. Kieber, A. Li, P. J. Seaton, *Environ. Sci. Technol.* **33**, 993–998 (1999).
41. J. Heil *et al*., *Geochim. Cosmochim. Acta* **139**, 72–82 (2014).
42. M. J. A. Rijkenberg *et al*., *Mar. Chem.* **93**, 119–129 (2005).
43. R. G. Zepp, J. Hoigne, H. Bader, *Environ. Sci. Technol.* **21**, 443–450 (1987).
44. T. Liu, J. Deng, C. Yang, M. Liu, Y. Liu, *Separ. Purif. Tech.* **304**, 122364 (2023).
45. H. A. Vanderploeg *et al*., *J. Great Lakes Res.* **50**, 102291 (2024).
46. S. Overmans *et al*., *J. Geophys. Res. Oceans* **127**, e2021JC017654 (2022).
47. X. S. Wan *et al*., *Nat. Geosci.* **16**, 29–36 (2022).
48. J. J. Beaulieu *et al*., *Proc. Natl. Acad. Sci. U.S.A.* **108**, 214–219 (2011).
49. A. R. McLeod, T. Brand, C. N. Campbell, K. Davidson, A. D. Hatton, *J. Geophys. Res. Biogeosci.* **126**, e2021JG006345 (2021).
50. J. Wang *et al*., *Environ. Sci. Technol.* **57**, 13506–13519 (2023).

ACKNOWLEDGMENTS

We thank J. Forja and T. Ortega for helping with gas chromatography analysis at the Department of Physical Chemistry of the University of Cádiz and G. Sánchez and L. Alados-Arboledas from the Applied Physics Department of the Andalusian Inter-University Institute for Earth System Research (IISTA-CEAMA) for providing the sunlight radiation data during the 2021 experiments. We also thank L. Bristow for measuring samples of experiments 7 and 8 and H. W. Bange for organizing the monthly Boknis Eck sampling campaign and providing the inorganic N measurements. We thank B. B. Ward for hosting E.L.-P. in 2018 and allowing her to use the mass spectrometer for experiment 9 measurements and for insightful comments and support during the review process. We also express our gratitude to the members of the Ward laboratory at Princeton University for their thoughtful comments on this manuscript. **Funding:** This study was supported by MNat - Consejería de Universidad, Investigación e Innovación, Junta de Andalucía, Spain, grant QUAL21-011 (I.R.); Spanish Ministry of Science, Innovation and Universities, grants RTI2018- 098849-B-I00 (I.R. and R.M.-B.) and MICIU/AEI/10.13039/501100011033 (I.R.); the European Regional Development Fund (ERDF), grant PID2022.1378650B.100 (I.R.); Spanish Ministry of Education, Culture and Sport, PhD grant FPU014/02917 (E.L.-P.); AEET-SIBECOL project for young researchers, grant PHOTON 2020 (E.L.-P.); Danmarks Frie Forskningsfond, grants 1026-00428B (C.L.) and 1127-00362B (B.T.); Carlsbergfondet, grant CF18-1071 (B.T.); and European Commission, Marie Skłodowska-Curie postdoctoral fellowship HORIZON-MSCA-2021-PF-01, grant 101066750 (E.L.-P.). **Author contributions:** Conceptualization: E.L.-P., I.R., R.M.-B., C.L., B.T.; Funding acquisition: I.R., R.M.-B., C.L., E.L.-P.; Investigation: E.L.-P., I.R., R.M.-B., B.T.; Methodology: E.L.-P., I.R., R.M.-B., B.T., C.L.; Project administration: I.R., E.L.-P., C.L.; Supervision: I.R., R.M.-B., C.L.; Visualization: E.L.-P.; Writing – original draft: E.L.-P.; Writing – review & editing: I.R., R.M.-B., B.T., C.L., E.L.-P. **Competing interests:** The authors declare that they have no competing interests. **Data and materials availability:** All data are available in the main text or the supplementary materials.

SUPPLEMENTARY MATERIALS

science.org/doi/10.1126/science.adq0302
Materials and Methods
Supplementary Text
Figs. S1 to S7
Tables S1 to S8
References (*51–60*)

Submitted 3 May 2024; accepted 4 February 2025
10.1126/science.adq0302